DESIGN OF AN EXPERIMENTAL SYSTEM FOR INVESTIGATION OF OXYGEN ATOM PRODUCTION IN A MICROWAVE DISCHARGE*

By

Jeffrey Robert Hinkle

A THESIS

Submitted to
Michigan State University
in Partial Fulfillment of the Requirements
for the Degree of

MASTERS OF SCIENCE

Department of Mechanical Engineering

1984

*Research Supported by NASA Grant No NSG3299

ABSTRACT

DESIGN OF AN EXPERIMENTAL SYSTEM
FOR INVESTIGATION OF
OXYGEN ATOM PRODUCTION IN A
MICROWAVE DISCHARGE

By

Jeffrey Robert Hinkle

This thesis describes, in detail, the experimental apparatus used to produce a microwave initiated plasma (2.44 GHz), as well as the equipment lay-out required to perform various diagnostic measurements. System integrity, flexibility, simplicity and control are discussed with the aim of minimizing equipment down time. Oxygen atom concentration, as a function of distance down stream of the discharge exit plane, was determined by titrating with nitrogen dioxide using a movable probe technique. It was found that an increase in power or a decrease in pressure resulted in higher concentrations of atomic oxygen at specific points downstream from the discharge. Flow rate had little effect on the overall production of atoms, but increasing the supply gas flow did result in increasing the oxygen atom yield (gm-atom/kw-hr). The largest dissociation measured was 70% at a pressure of 12 torr, a flow rate of 0.4 cc/sec and 500 watts of absorbed power.

DEDICATION

To Cecily, Lauren and Christin

ACKNOWLEDGEMENT

I am pleased to acknowledge the guidance of my major professor and advisor Dr. Ronald L. Kerber. I am grateful to have had the opportunity to work on this project with Dr. Mary L. Brake; for not only her efforts in the many hours of data collection and reduction, but also for her continued encouragement. I wish also to thank Mrs. Jeannie M. King for the many hours that she devoted to preparing and revising this manuscript. Finally, I wish to acknowledge that the successful completion of this thesis, indeed my entire undergraduate and graduate program, would not have been possible without the patience, understanding, faith and enthusiasm of my wife, Cecily.

TABLE OF CONTENTS

LIST OF TABLES

LIST OF FIGURES

CHAPTER 1, INTRODUCTION
1.1 The Experiment 1
1.2 Previous Work 6

CHAPTER 2, EXPERIMENTAL APPARATUS
2.1 Oxygen Supply System 9
2.2 Plasma Containment Tubes 11
2.3 Power Coupling System 12
2.4 Analytical Flow Regime 15
2.5 Pressure Control System 16
2.6 Vacuum System 17

CHAPTER 3, DIAGNOSTICS
3.1 Titration 18
3.2 Spectroscopy 20
3.2.1 Atomic Emission 20
3.2.2 O_2 ($^1\Delta_g$) Infrared Emission (1.27 μm) 22
3.2.3 Stark Broadening 23

CHAPTER 4, DISCUSSION
4.1 Gas Flow System 25
4.2 Plasma Discharge 25
4.3 Resonant Cavity 28
4.4 Titration System 28
4.5 Emission Spectra 30
4.5.1 Visible 30
4.5.2 Infrared 31
4.5.3 Stark Broadening 32

CHAPTER 5, RESULTS
5.1 Observations 35

CHAPTER 6, CONCLUSIONS
6.1 Summary 40
6.2 Comparison of Experimental Method 40
6.3 Proposal for Additional Research 41
6.3.1 Analytical 41
6.3.2 Experimental 42

REFERENCES 43

TABLES 46

FIGURES 49

LIST OF TABLES

Table 1 - Observed Spectral Lines of Atomic Oxygen.

Table 2 - Observed Band Heads of The First Negative System of O_2^+.

Table 3 - Calculated Resonant Cavity Modes for an Evacuated Cylinder (178 mm ID)

LIST OF FIGURES

Figure 1 - Experimental Apparatus

Figure 2 - Movable Titration Probe

Figure 3 - Plasma Containment Radial Flow Tube

Figure 4 - Plasma Containment Tube Adaptor - Window

Figure 5 - System Isolation Valve (V-2)

Figure 6 - O_2 ($^1\Delta_g$) Detection Cavity

Figure 7 - Nitrogen Dioxide Gas Supply System

Figure 8a & b - Nitrogen Dioxide Gas Titration Station

Figure 9a & b - Observed Plasma Spatial Distributions

Figure 10 - The Effect of Distance on P_{NO_2} for Several Pressures

Figure 11 - Molecular Conversion vs Distance From the Exit of the Reactor Cavity for Various Pressures

Figure 12 - Molecular Conversion vs Distance for Various Flowrates

Figure 13 - The Number of Atoms Per Unit Energy (Yield) Produced vs Distance

Figure 14 - Oxygen Atom Yield and Molecular Conversion vs Flowrate

Figure 15 - The Effect of Power on Oxygen Atom Yield and Oxygen Molecule Conversion

CHAPTER 1

INTRODUCTION

1.1 The Experiment

Several investigators have successfully produced oxygen discharges in a variety of experiments[1-5]. The generation of oxygen atoms as a function of flow rate, power and pressure has been analyzed by various techniques. A particularly common technique of determining oxygen atom production is by titration, using nitrogen dioxide as the titrant.

The titration analysis conducted in References 1-5 were performed at one, two or three fixed locations some distance from the exit of a discharge. Pressure ranges of 0 to 10 torr, flow rates of 0.2 to 17.6 cc/sec and absorbed power of 0 to 400 watts were reported.

The objective of the work presented in this paper was to investigate the production of oxygen atom generation within a microwave discharge and to maximize free oxygen atom production as a function of distance. The distance was measured from the exit of the microwave discharge to the downstream location at which the titration was performed. These measurements served as reference data for the purpose of verifying a computer-generated kinetic model[6].

This paper describes, in detail, the experimental apparatus used to produce the microwave discharge, as well as various diagnostic procedures. In all, five separate and distinct analytical techniques were

utilized. They were:

1. Emission spectroscopy (3000 to 7500 Å) to measure electronic state and ion concentrations.

2. Chemical titration to measure oxygen concentration.

3. Infrared emission spectroscopy to measure $[O_2\ (^1\Delta_g)]$.

4. Stark broadening to measure n_e.

5. Visual observations to detect extent of plasma and flow bypassing.

It will be shown that the varying degree of success of these analytical techniques, coupled with the necessary design configurations required to support them, lend credit to the simplicity and economy of the chemical titration analysis.

Due to the varied nature of the experimental techniques, the overall flexibility in design and layout of the experimental apparatus was of primary importance. The collection of spectroscopic data (both visible and infrared), the employment of a novel titration technique, the ability to perform radial and axial plasma observations, the flexibility to examine alternate flow configurations, and the anticipation of performing Stark broadening measurements presented formidable design constraints (see Figure 1).

Oxygen plasma emission spectra was collected over the range of 3000 to 7500 Å with the goal of identifying plasma composition. The emission spectra was compared to standard emission tables[7]. Primarily, atomic neutral oxygen lines were observed. Only under special conditions were vibrational and rotational molecular band structures observed (see Tables 1 and 2).

Several attempts were made at measuring the O_2 ($^1\Delta_g$) emission (1.27 μm) downstream of the oxygen plasma. It was anticipated that the measured radiance could be related to the physical processes involved. Repeated efforts, under various conditions, were unsuccessful in producing the sought for signal. The sensitivity of the detector, D^*, over the range of interest, for the particular experimental apparatus, was determined to be 1.6×10^{12} cm(Hz)$^{\frac{1}{2}}$/watt.

Nitrogen dioxide titration has proven to be of fundamental importance when determining free oxygen atom production in molecular oxygen dissociation[1-4]. One very important goal of this experiment was to generate a continuous profile of the percent of molecular gas dissociated as a function of distance. This distance was measured from the exit plane of the inductively coupled plasma to specifically chosen cross-sectional planes within the recombination zone. The cross-sectional plane was defined by radially injecting nitrogen dioxide titrant within the effluent gases. This goal was established in an attempt to resolve the discrepancies observed in References 1-3. Battey's[1] results indicate that atomic oxygen concentrations were independent of the molecular oxygen flow rate, whereas Bell[2] and Mearns[3] found that increased flow rates increases conversion.

Additionally, the large number of possible variables (i.e., flow rates, discharge resident time, pressure, power coupling mode, absorbed power and chemical reaction rates) seemed to suggest that the recombination chemical kinetics may not exhibit a simple relation; consequently, extrapolation techniques could be misleading at or near the discharge exit plane.

In order to overcome the fixed probe limitations, movable axial probes were designed which delivered the titrant at the desired location. The probe tip was positioned along the centerline (axis) of the discharge flow tube with a 43 cm travel (see Figure 2). This provided two primary advantages: 1) it maximized reagent mixing by injecting the nitrogen dioxide radially within the laminar oxygen flow stream (R_e = 8) and, 2) it provided titration analysis at any particular cross-sectional plane downstream of the oxygen plasma discharge. This titration regime included the resonant cavity exit plane; consequently, free oxygen atom determination at, or near, the plasma exit plane was made possible. This proved to be an important advantage over other experimental methods where fixed titration ports were utilized, since most of the recombination kinetics occur within the first few centimeters of travel downstream of the discharge.

The employment of a screened window located on the side of the cylindrical reactor cavity[8] provided the means for directly observing plasma dimensions and characteristics. This, however, lead to the misconception that the plasma uniformly filled the quartz containment tube. The installation of an axial window provided plasma observation along the center line of the containment tube. Visual (on axis)

observations revealed several non-uniform plasma configurations. These spatial distributions suggested the possibility of the supply gas by-passing the plasma discharge. These characteristics were pressure and power dependent for each cavity configuration (probe and short positions) and were attributed to the plasma changing electromagnetic modes of operation. To resolve these variations in plasma density and improve dissociation ratios, several plasma containment tubes were investigated. These varied in radius and flow configurations. Large radius flow tubes (37 mm I.D. and greater) proved difficult to work with, due to the excessive amounts of microwave radiation leakage; as a result, these studies were limited. One of the characteristic modes which was observed at high power and high pressure was a high density right circular plasma cylinder whose centerline was coincident with the axis of the quartz containment tube. The center of the right circular plasma cylinder did not support a visible plasma, which made the on-axis view of the plasma appear annular. A radial flow tube[13] was designed and employed in order to eliminate the possibility of the supply gas tunneling through this self-shielded region of the plasma. The radial flow tube directed the flow of excited gasses away from the exterior surfaces towards the containment tube centerline (radial), prior to exiting the discharge (see Figure 3). Although this method appeared to address the tunneling problem, it did not solve the self-shielding phenomenon which was responsible for the tunneling effect in the first place. Additionally, the design concept proved to be flawed, in that the radial flow path was generated by pinholes through which the gas would flow. Subsequent titration indicated that little or no atomic oxygen was detectable downstream of the discharge. It was postulated

that surface recombination kinetics was the principal factor governing these results.

The successes of Stark broadening measurements as a diagnostic tool[9,10,11] for high pressure/high density plasma analysis lead to its application in the present text. The capability of measuring the broadening of the hydrogen β-line (4861 Å), due to the Stark effect, could provide an important contribution to the detemination of electron density calculations. At present, difficulties exist in establishing signal readout and is the subject of ongoing research.

1.2 Previous Work

Many researchers have examined different ways to produce atomic oxygen from molecular oxygen. They have used positive column discharges, radio-frequency discharges and microwave discharges.

P. Kocian[12] examined a positive column discharge. The discharge was produced in a pyrex tube 6.0 cm in diameter and 80 cm in length. He varied the pressure from 0.1 to 2 torr and the current from 20 to 150 mA, with a constant oxygen flow rate of 2 cc/sec. The atomic oxygen concentration was measured with a catalytic probe. Under this technique, a catalyst (platinum wire) was introduced into the atomic oxygen flow stream. The probe provides a site for high rate surface recombination kinetics. The oxygen atom flux is measured by correlating the release of energy from the surface recombination to a change in electrical resistance of the probe as a result of an increased temperature.

The highest degree of dissociation was found to be 10% at 150 mA and 1.5 torr.

J. Battey[1] dissociated oxygen molecules using a radio frequency discharge (13.56 MHz) in a 20.3 cm diameter cylindrical quartz tube, 33 cm in length. The flow rate varied from 1.67 to 15 cc/sec, the pressure ranged from 1 to 3.0 torr, and the power varied from 0 to 200 watts. He measured oxygen atom concentration by titration with NO_2. The maximum conversion 0_2 to 0 atoms was 7.5% at 0.5 torr and 200 W.

A. Bell and K. Kwong[2] also studied a similar radio-frequency discharge at 13.56 MHz, varying the power from 0 to 140 watts, ranging the pressure from 2 to 4 torr and varying the flow rate from 2×10^{-4} to 1×10^{-3} moles/min. Their reactor was a pyrex pillbox of 8 cm diameter and 2.5 cm high. They detected the production of oxygen atoms by NO_2 titration. The highest conversion observed was 23% at 2 torr for a power of 74 watts and a flow of 6.30×10^{-4} moles/min.

A. Mearns and A. Morris[3] studied oxygen atom production in a 2.45 GHz microwave discharge. The first reactor consisted of a coaxial cavity with a plasma volume of 2.1 cc and a power range of 3 to 200 watts. The second reactor consisted of a cylindrical cavity with a plasma volume of 67 cc and a power range of 700 to 2000 watts. The discharges were contained in a 1 cm diameter tube. Discharge pressure was examined from 9 to 10 torr and the absorbed power ranged from 0 to 400 watts. The highest 0_2 dissociation measured was 14% at 2 torr and

200 watts in a silica tube. NO_2 titration at three fixed positions outside the discharge was used to determine oxygen atom production.

Bell and Kwong, Mearns and Morris, and Battey agree that increased pressure decreases conversion, but Battey's results indicate that atomic oxygen concentrations are independent of the molecular oxygen flow rate whereas Bell and Mearns find that increased flow decreased conversion. Bell concludes that oxygen atom yield is insensitive to flow whereas Mearns finds that oxygen yield decreases with flow. In this paper, some of these discrepancies are addressed.

CHAPTER 2

EXPERIMENTAL APPARATUS

2.1 Oxygen Supply System

Research grade oxygen (99.993% minimum purity) was used as the supply gas without additional purification or moisture removal. From the oxygen bottle gas regulator, the oxygen flowed through a back-pressure regulator (Matheson, Model Number 70A), a supply gas isolation valve (Whitney, Part Number SS-43-S4), a high capacity strainer (Nupro, Model Number SS-4TF-7), a rotometer gas flow indicator (Matheson, Part Number 601) and a bellows fine metering valve (Nupro, Part Number SS-4BMW). Located between the supply gas isolation valve (O-1) and the high capacity strainer was an atmospheric vent line and isolation valve (O-2) (Nupro, Part Number SS-4H). Located between the supply gas strainer and the rotometer was a Heise gauge (0-1600 mm Hg, Model Number C-63802). The Heise gauge was used to indicate supply gas back-pressure. The back-pressure regulator maintained a constant O_2 supply pressure of 1400 mm Hg. This pressure was chosen as a convenient value which would provide an adequate pressure-head, above atmospheric pressure, in order to minimize the total quantity of equipment exposed to sub-atmospheric pressures during operation. The high capacity strainer was selected and positioned to protect the Heise gauge, rotometer and metering valve by filtering out particulate (greater than 7 microns) from either the vent line or oxygen supply system (see Figure 1).

Since the Heise gauge is bourdon tube (subject to atmospheric pressure variations) prior to use, calibration was necessary. This was accomplished by (see Figure 1):

1) Closing the supply gas isolation valve (O-1)

2) Closing the atmospheric vent isolation valve (O-2)

3) Fully opening the oxygen metering valve (O-3)

4) Opening the vacuum pump isolation valve (V-1), and

5) Starting the vacuum pump.

Once the rotometer indicated no further evacuation (zero flow), the Heise gauge was adjusted to match a McLeod gauge. The primary purpose of the McLeod gauge was to determine plasma pressures during operation; however, under zero flow conditions and proper valve lineup, these pressure instruments should read the same. Once the Heise gauge adjustment was completed, barometric pressure could be determined by:

6) Closing the oxygen metering valve (O-3), and

7) Cracking the atmospheric vent isolation valve (O-2)

The Heise gauge would then indicate atmospheric pressure. Once the barometric pressure had been determined, the oxygen supply was brought on line-by:

8) Closing the atmospheric vent isolation valve (0-2)

9) Slowly opening the supply gas isolation valve (0-1)

This would bring the oxygen supply system up to the 1400 mm Hg setting. Oxygen was normally supplied up to the supply gas isolation valve (0-1) during this evolution to preclude the possiblity of exposing the back-pressure regulator and sub-atmospheric pressures.

Oxygen was supplied to the various quartz containment tubes through a flexible male connector hose (Swaglok Part Number SS-400-1FH(1/4L)-4-316) coupled to either a tapered quartz containment tube or a specially designed adaptor-window.

2.2 Plasma Containment Tubes

Axial and radial flow configurations (within the discharge) were investigated using two axial flow tubes and a single radial flow tube. In all cases, the quartz containment tubes were positioned at the resonant cavities centerline. The two axial flow tubes were a simple pipe design (18 mm and 37 mm I.D., 1 meter long). The 18 mm quartz flow tube was equipped with a smooth taper so that it would accept the 6.4 mm oxygen supply line. The 37 mm quartz flow tube was fitted with a special adaptor-window (see Figure 4) so that cross-sectional plasma observations could be made by looking down the plasma containment tube centerline. The adaptor body was fabricated from 51 mm aluminum bar stock, 31.8 mm long. One end was recessed 25 mm to accept the 37 mm I.D. quartz tube. A 25.4 mm hole was bored through the centerline and

the remaining end was fitted with an "O"-ring, a pyrex window and a retaining ring. The retaining ring was fastended to the adaptor body using four cap screws (3/4 in x 6-32). The side of the adaptor was bored and threaded to accept a 6.4 mm pipe nipple. The 6.4 mm threaded pipe connection served the oxygen supply line flexible male connector hose (Swagelok Part Number SS-400-1FH(1/4L)-4-316).

A 46 mm I.D. radial flow tube was constructed by fusing a quartz "test tube" like insert to an outer quartz sleeve. The length of the insert was perforated with small diameter pin holes (approximately 0.5 mm diameter) which provided radial flow distribution with the resonant cavity (see Figure 3). The radial flow tube was installed so that the higher pressure was established on the outside of the sleeve (up stream side) and lower pressure on the inside. The flow configuration being radial, from the outside of the flow tube towards the centerline. The idea was to force the thin skin layer discharge towards the center, into the lower pressure zone, where third body collisional deactivation would be less probable. As a result, the dissociation efficiency would therefore increase at the exit plane of the resonant cavity.

The number of penetrations and the pumping capacity limited the differential pressure which could be realized across the radial flow tube to less than 5 torr. Earlier, this concept had been used successfully by Kerber and McKnight[13] with systems of higher pumping capacities.

2.3 Power Coupling System

A commercially available 2.44 GHz magnetron oscillator (Litton Part Number 705009) was used as the microwave power source. The magnetron was rated at 1000 watts of continuous power. A variable water-cooled attenuator (Raytheon Model Number SAVK-10) was employed to provide an available power range of 200 to 800 watts at the resonant cavity. The magnetron was protected from reflected power by use of a circulator and a matched load. Just prior to the microwave power entering the resonant cavity, a directional coupler (MICROLAB/FXR Model Number 5612D) was installed, so that incident and reflected power could be monitored simultaneously. The power monitoring system consisted of two (2) power sensors (Hewlett-Packard Model Number 8481A), two (2) 30 db alternators (Microlab/FXR Model Number AD-30N) and two (2) power meters (Hewlett Packard Model Number 435A) operating in parallel. Care had been exercised to calibrate the power meters, attenuators, and directional coupler, as a matched unit, against a known standard. The net power delivered to the cavity was taken as the incident power minus the reflected power, as read from the power meters. In this manner resonant cavity modes were readily established. All of the experimental data was collected where reflected power was a minimum. Typically reflected power was less than 5% of incident power. Table 3 lists calculated cavity modes as a function of cavity length, based on an evacuated cylinder of 17.8 cm in diameter.

Microwave power was delivered to a movable coaxial probe by a rectangular wave guide. A rectangular-to-coaxial wave guide converter coupled the coaxial probe to the microwave source. The center conductor

of the coaxial probe was of fixed length which moved in and out of the resonant cavity (see Figures 1 and 3). This provided a means, in conjunction with the sliding short, to optimally tune the resonant cavity, thereby minimizing reflected power.

The resonant cavity[8] was fabricated from 17.8 cm (nominal) brass tubing with an overall length of 30.5 cm. The tube section was capped on both ends and fitted with a sliding short. The sliding short was a brass disk which contained a band of "finger contacts" which completed the electrical circuit to the walls of the cylindrical cavity. The relative position of the sliding short varied the effective length of the resonant cavity. Under these conditions, the resonant cavity effective length could be varied from 5 to 16 cm. The cavity was equipped with a screened window (51 mm square), located on the side of the cylindrical cavity, opposite the coaxial wave guide probe. This window was used to collect spectral and visual information (see Figures 1 and 3).

Auxiliary cooling was supplied to the cavity by two methods: 6.4 mm copper tubing was soldered to the outside of the cylindrical cavity, and on the back side of the sliding short. Tap water was circulated through the tubing to dissipate the heat. Additionally, forced air was supplied to the inner region of the cavity to convectively cool the surface of the quartz tubing.

2.4 Analytical Flow Regime

The downstream ends of the various containment tubes were fitted with a 50/50 mm ground quartz flare. This flare was mated to a 50/50 mm ground pyrex taper to achieve a strong and inexpensive quartz to pyrex joint. Changing plasma containment tubes could be effected by simply breaking vacuum and switching tubes (the pyrex taper was common to each containment tube). The ground pyrex taper was joined to the remaining 51 mm I.D. conical piping system by fusing it to a pyrex tee (Corning Part Number 72-8250). The opposite end of the tee was fitted with a flange and a 6.4 mm Cajon Ultra-Torr male connector (Part Number SS-4-UT-1-4) (see Figure 2). The Ultra-Torr fitting was bored out to provide sufficient clearance to permit relative motion between the fitting and a 6.4 mm pyrex titration probe. The branch connection, on the tee, was joined to another branch connection of an identical tee, such that the two tee sections formed a rotated "H" configuration. One of the remaining ends of the second tee was flanged-off, creating a dead leg. The flange was fitted with a 6.4 mm street tee (Cajon Part Number SS-4-ST) in which the through-connection was bored out to 8 mm I.D. to permit manual operation of a simple plug valve, whose valve stem passed though the center of a street tee connector (see Figure 5). The female through-connection was fitted with an Ultra-Torr male connector (Cajon Part Number SS-4-UT-1-4) which in effect, served as a valve stuffing box and seal assembly. The stainless steel (6.4 mm) valve stem and the teflon seat and disk were fabricated and installed in such a way that the valve seat was sandwiched between the second tee and the remaining flow system. The use of this valve (V-2) provided a positive seal between the analytical regions of the flow system and the vacuum system.

This was necessary since the titrant (NO_2) flow determination was based on the time rate of change of pressure in an isolated volume (dP/dt). This design permitted titration measurements, and titrant flow determinations, to be performed under identical flow conditions. The purpose of this procedure was to eliminate the error introduced by switching the titrant flow path (through an alternate flow configuration) when performing flow rate measurements.

The remainder of the flow system was followed by a 122 cm pyrex conical tube (Corning Part Number 72-7220) connected to another tee (Corning Part Number 72-8250). The through-connection of the third tee was fitted with a flat pyrex window. This created a cavity which measured 172 cm in length and 51 mm in diameter. The purpose of this cavity was to provide a sufficiently long optical path such that detection of the $O_2(^1\Delta_g)$ emission would be probable. The effective length of the cavity was doubled (345 cm) by placing a mirror on the end opposite the detector window. Borosilicate was chosen as the window material due to its availability and transparency in the 1.27 μm region (see Figure 6).

2.5 Pressure Control System

The system pressure control gas was designed and used to bleed oxygen into the suction side of the positive displacement vacuum pump (see Figure 1). This proved to be an effective means of controlling system pressure. Control gas was supplied from a gas cylinder regulator (20 psig) to a fine metering valve (Nupro Part Number SS-4-MG). Throttling of the fine metering valve would permit rapid and repeatable

adjustments to system pressure. This, in effect, de-coupled the research oxygen supply gas (flow rates) from controlling system pressure. The ability to vary oxygen supply flow rates at fixed system pressure was critical to resolving discrepancies as reported in References 1-3. Commercial grade oxygen was chosen as the control gas due to its compatibility, availability and cost.

2.6 Vacuum System

The vacuum system consisted of a fourth tee (Corning Part Number 72-8250) whose through-connection served as the system pressure control gas port, while the branch-connection was coupled to the vacuum pump suction line (see Figure 1). The suction line contained a high capacity liquid nitrogen cold trap and a flexible vibration isolation lead. The stainless steel flexible lead minimized the amount of vibration transmitted to the flow system and allowed for stress relief due to misalignment between the vacuum pump and the rigid pyrex flow system. The pump was a single-stage rotary piston vacuum pump (Beach-Russ Co Model Number RP-50-D) with a design capacity of 37.75 liters per second at one atmosphere.

CHAPTER 3

DIAGNOSTICS

3.1 Titration

Due to the extreme toxicity of nitrogen dioxide gas, special handling of the titration flow system was required. The majority of the titration system was maintained within a fume hood. The nitrogen dioxide gas handling system outside of the fume hood was kept at a sub-atmospheric pressure. This was a preventive measure in the event of system failure (i.e., leaks). The nitrogen dioxide flow system consisted of a supply gas cylinder with an integral isolation valve, a fine metering valve (Nupro Number SS-4MG), and a line isolation valve (Nupro Number SS-4H) feeding a pyrex reservoir. The reservoir was constructed from a one-foot section of straight conical pyrex pipe (Corning Part Number 72-7190), wherein one of the ends had been sealed off to form a large "test tube". This "test tube" served both as a liquid trap and a constant temperature reservoir (see Figure 7). The NO_2 supply line entered through the top of the cylinder, which was capped with a stainless steel flange. The flange contained two male connectors (Swagelok Part Number SS-400-1-4), wherein one had been bored clear through to permit the passage of a 6.4 mm stainless steel supply line. The supply line extended to the bottom of the reservoir which served as a nitrogen dioxide fill line. A limited quantity of liquid nitrogen dioxide was admitted to the reservoir, after which the supply cylinder was isolated. The reservoir was partially emmersed in a constant temperature bath in order to maintain the liquid-vapor saturation equilibrium at the desired

temperature and pressure. This configuration provided two distinct benefits: (1) personnel safety; operating procedures limited the total quantity of potentially hazardous gas to a minimum, and (2) it effectively maintained the nitrogen dioxide at a constant back-pressure during analysis (less than one atmosphere). The nitrogen dioxide vapor was drawn off the top of the reservoir through the remaining male connector, through an isolation valve (Nupro Part Number SS-4MG), and delivered to the titration station (see Figure 8a). The titration station consisted of an isolation valve T-1 (Nupro Part Number SS-4UG), a fine metering valve T-2 (Nupro Part Number SS-4GMW), a second isolation valve T-3 (Nupro Part Number SS-4UG), and a flexible hose which supplied nitrogen dioxide to the titration probe. Between valves T-1 and T-2 was a tee (Swaglok Part Number SS-400-3) which was connected to an isolation valve T-4 (Nupro Part Number SS-4H). Between T-2 and T-3 was another tee and isolation valve T-5 (Nupro Part Number SS-4H). These two valves T-4 and T-5 were connected to a common gauge (Penwalt Wallace & Tieinan, 0-50 mm Hg, Model FA160), which was used for absolute pressure indication. This common line contained a known surge volume which was required to perform flow rate determination in terms of time rate of change of pressure (dP/dt). Several flow configurations could be achieved depending upon the positions of T-2, 3, 4, and 5. The normal configuration was: throttling with T-2; T-1, 3 and 5 full open, T-4 shut. When the titrant flow rate determination was desired, T-3 was shut and T-4 opened. The gas was directed into the known isolated volume. A swift hand watch and the absolute pressure gauge provided the necessary information for the time rate of change pressure data. This system was later modified when the standard volume became the oxygen flow system itself (see Figure 8b). In the later case, T-5 was directly

connected to the oxygen flow system and surge volume was removed. Under these conditions, the flow configuration was: Throttle with T-2; T-1, 3 and 5 fully open, T-4 shut. When the flow rate determination was desired, the upstream half of the oxygen flow system was isolated and the dP/dt measurement was taken directly. Thus the titration system was simplified, reducing the number of possible errors and simplifying the overall measurement technique.

The nitrogen dioxide gas titration probes measured 6.4 mm in diameter and 86 cm in length. The tip of the probes were rounded-off and punctured with eight radial holes approximately 1 mm in diameter. The holes formed a ring, in a single cross-sectional plane, located 3 mm back from the end of the probe. As such, the nitrogen dioxide would flow within the titration probe, and exit in a radial fashion, defining a cross-sectional plane near the tip of the titration probe. The nitrogen dioxide mixed with the effluent plasma discharge gases in a cross-flow pattern (see Figure 2). This configuration maximized reagent mixing, and provided the means to determine a continuous "recombination profile" of the free oxygen atoms downstream of the discharge.

3.2 Spectroscopy

3.2.1 Atomic Emission

Direct viewing of the oxygen plasma emission spectra was made possible with the aid of the 51 mm square window located in the side of the resonant cavity. An archromatic collecting lens (Oriel Part Number A-18-161-66) with a focal length of 160 mm and an f/3.2 was used to

produce a real image of the oxygen plasma at the monocromator's entrance slit.

A one meter Czerny-Turner Grating Scanning Monochromator (Spex Model Number 1704) was used to collect and isolate the spectral information. The monochromator had a maximum theoretical resolving power of 0.08 Å when equipped with the 1,200 groves/mm ruled grating. The radiant energy was collected and converted to an electrical signal using a high quantum efficiency Photomultiplier Tube (EMI-Gencom Model Number 9658R). The photomultiplier was mounted in a forced air thermoelectric cooled housing unit (EMI FACT-50 Mk III) capable of cooling the photomultiplier tube down to -30°C. The cooling unit effectively reduced the photomultiplier dark current from 7.6×10^{-9} amps to 5.0×11^{-11} amps at -30°C. The photomultiplier tube was negatively biased (-890 Volts DC) with a regulated high voltage power supply (EMI Gemcon Model Number 3000R). The photomultiplier signals were converted to digital readout using a 3½ digit picoameter (Keithlay Model Number 480). An external inverting analog output permitted strip chart recording from the current to voltage converter. The strip chart recorder (ACCO Bristol, Dynamaster Model Number 71A/4PG/PG/PG/PG/591-51-TE142B-T7554) was equipped with multi-channel capabilities which permitted simultaneous spectrum recording and automatic wavelength indexing. Voltage converters (current limiting) interfaced the input signals to the strip chart recorder.

As part of the precautionary measures to ensure signal quality, normal operations required the laboratory to be darkened and all extraneous light sources eliminated. The complete optical diagnosis system was mounted on a vibration isolation table (Newport Research Model

Number RS-46-18) supported on four pneumatic isolation mounts (Newport Research Type YL-A). Additionally, the rotary vacuum pump was mounted on commercially available vibration isolation mounts. During spectroscopic scanning, all system parameters were closely monitored to ensure constant conditions throughout the evolution.

3.2.2 $O_2(^1\Delta_g)$ Infrared Emission (1.27 μm)

The effective 345 cm long $O_2(^1\Delta_g)$ emission cavity was sealed on one end with a polished aluminum plate and on the other with a borosilicate window. Immediately following the window was a collecting lens with a focal length of 200 mm and an f/3.94 (Oriel Part Number A-18-200-66). Between the lens and its focal point was a mechanical light chopper (Princeton Applied Research Model Number 125A). An InSb LTO Photovoltaic Detector was placed at the focal point of the collecting lens (see Figure 6). The detector was supplied by Santa Barbara Research Center (Model Number C039/40742) with a D* of 2×10^{11} cm$(Hz)^{\frac{1}{2}}$/watt. At the mirrored end of the cavity (upstream) a black body source (Infrared Industries Model Number 101B/464) was used to align the infrared system and to verify signal readout. The modulated signal was phase-matched to the chopped frequency using a lock-in amplifier (Princeton Applied Research Model Number 128A). The lock-in amplifier provided direct signal strength readout which was interfaced with the strip chart recorder.

3.2.3 Stark Broadening

The Stark Broadening measurement was initially complicated by the fact that the plasma was an extended source which was remotely located; in the sense that it was contained within the resonant cavity. Fundamental to the employment of a Fabry-Perot interferometer is the collimation of light. Typically, a point source is used, which is located at the focal point of the collecting lense. Since a pin hole could not be located on the extended source (plasma containment tube), an imaging lens was required to produce a real image of the plasma at a plane outside the resonant cavity (see Figure 1). An imaging lens (with a focal length of 60 mm and a f/0.69) produced a one-to-one image of the plasma on a pin hole 240 mm from the plasma centerline (by placing the lens midway between plasma and the pin hole). The pin hole was followed by a collimating lens (Oriel Part Number A-18-161-66) and the Fabry-Perot interferometer (Burleigh Model RC-110).

The mirrors (Burleigh RC-670, R=97.5%, 450-550 nm) used in the Fabry-Perot interferometer were chosen to be preferential towards the Hydrogen β-line (4861 Å). Upon exiting the interferometer, the light passed through a focusing lens which focused the light onto the monachromators entrance slit. The focusing lens F-number was chosen to match the monachromators (f/9.0). The monachomator was followed by previously described transducer, current to voltage converter, and data recorder (see Figure 1).

A programmable ramp generator (Burleigh Model Number RC-45) provided final mirror alignment and variable ramp capabilities. These

capabilities included varying the ramp magnitude and duration. The programmable ramp generator was equipped with an external ramp signal output. This output was simultaneously monitored with the analytical signal by either a dual beam Oscilloscope (Tektronix Model Number 7844) or the multi-channel strip chart recorder.

CHAPTER 4

DISCUSSION

4.1 Gas Flow System

Since the experimental apparatus (see Figure 1) was operated at sub-atmospheric pressures, system integrity was of primary importance. The guidelines adopted to ensure system integrity and maximum reliability were to minimize unions whenever possible and to utilize flexible connector hoses at critical design locations. The flexible connector hoses alleviated misalignment stresses and reduced the total amount of vibration transmitted to the pyrex/quartz flow system.

From previous work[1,4,12,14&15] it was known that surface recombination plays an important role in free oxygen atom quenching. By maximizing laminar pipe flow and eliminating turbulence (vorticity induced at pipe bends), surface recombination kinetics should have been gas diffusion limited. Therefore, straight runs of pipe (pyrex) of large diameters, were utilized wherever possible. Additionally, pumping capacity (vacuum) was maximized and pressure gradients were minimized throughout the gas flow system with the large diameter flow tubing.

4.2 Plasma Discharge

The use of the cylindrical resonant cavity[8] provided many important advantages over fixed geometry cavities[1-5]. The single most important advantage of the tunable cavity was the ability to couple

power into the plasma using several different electromagnetic modes (see Table 3). Cavity tuning was accomplished by selectively positioning the coaxial wave guide center conductor (probe) within the cavity and carefully adjusting the cavity length (by varying the sliding short position). The necessity to "tune" the cavity was largely a result of varying the plasma pressure and plasma dimensions (containment tubes). Impedance matching between the coaxial wave guide and the coaxial resonant cavity with the various diameter plasma containment tubes was not optimal. The impedance mismatch occurs as a result of a compromise between the ability to investigate various plasma dimensions and the idealized dimension. This compromise is largely justified by the ability to tune the cavity, such that reflected power is typically less than 5% of the incident power throughout the investigations. Optimized impedance matching required a 44 mm I.D. plasma containment tube. The approach to this optimized dimension was evident when the cavity was fitted with the 37 mm I.D. plasma containment tube. At pressures below 2 torr, the plasma completely filled the one meter long 37 mm I.D. containment tube. The plasma was bright white in color and reflected power was an absolute minimum. Some plasma extension had been observed with the smaller diameter tube (18 mm), but not to the extent described here.

The large diameter (37 mm I.D.) tube was equipped with an on-axis window for visual observations (see Figure 4). This was the first containment tube which was sufficiently large to observe cross-sectional plasma density variations (see figure 9). Although pressure tuning is a well known phenomenon, this tube was observed to switch electromagnetic modes during operations. By allowing the plasma pressure to sweep a narrow

range (one torr), at a fixed power input, several spatial distributions were observed. At low pressure (less than 0.5 torr) and minimum power (less than 400 watts) the plasma exhibited a spheroid shape not completely filling the containment tube. The plasma was a deep reddish-purple with the highest visible density nearest the power input probe. For power in the range of 400 to 800 watts and pressures of less than 8 torr the plasma would switch electromagnetic mode in an orderly fashion. The sequence was always the same, only the pressure bands at which the transition occurred would change. The transition pressure bands would progressively move to higher and higher ranges as power was increased. The sequence was as follows: At low pressures (less than 0.5 torr) the plasma uniformally filled the containment tube, both axially and radially. As pressure was increased above 0.5 torr the plasma became annular, when viewed on axis. At 0.7 torr the plasma split, on the side opposite the coaxial wave guide probe, to exhibited a saddle-like shape (horse shoe if viewed on axis). As pressure was further increased (1 to 8 torr), the saddle shape receded towards the probe side of the cavity. At pressures of 8 torr and greater, the plasma exhibited the same characteristics described above for low pressure and minimum power. As pressure was increased to 50 torr and beyond, the plasma collapsed towards the coaxial wave guide probe, exhibiting neither annular or centroidal characteristics. At an estimated 80 torr the plasma extinguished.

An additional peculiarity which was observed with this tube was that under certain conditions, moving the sliding short position 0.8 mm would cause the plasma to jump from one side of the containment tube to the other (180° out). The plasma would exhibit the same spatial

distribution (horse shoe), with simply a mirror image transition. These spatial distributions were only observed within the 37mm I.D. containment tube, however it emphasizes the need to exercise caution during data collection.

4.3 Resonant Cavity

It was customary to provide air and water cooling to the cavity at all times, since some microwave energy was constantly being lost to the resonant cavity walls during operation. The exterior cooling coils, which used liquid to cool the resonant cavity, proved to be somewhat problematic. The cooling medium utilized was tap water. The tap water temperature was approximately 13°C. Periodically, operating under humid conditions (summer months), a thin film of condensation would collect within the cavity. This eventually lead to air conditioning the laboratory. The condensation had a tendency to promote arcing between surfaces. The majority of the heat gain and arcing was experienced by loose fitting collars. The collars were split rings which were designed to accommodate the various sizes of the containment tubes. As a result of the arcing problems, these collars were later replaced with solid collars which were soldered in place. This eliminated the clearance gap where the majority of the arcing took place, with some loss of flexibility in the experimental apparatus.

4.4 Titration System

Free oxygen atom concentrations were determined by nitrogen dioxide titration. The nitrogen atom titration process is based on the following reactions:

$$O + NO_2 = NO + O_2 \qquad (1)$$

$$O + NO = NO_2 + h\nu \qquad (2)$$

In reaction one (1), free oxygen atoms exiting the plasma discharge are scavenged by the nitrogen dioxide molecules (see Figure 2). Reaction one (1) is very fast and is five (5) orders of magnitude faster than reaction two[6]. If the initial free oxygen atom production exceeds the rate at which nitrogen dioxide is being introduced, then reaction two follows. In reaction two, the remaining oxygen atoms (atoms not scavenged in reaction one) oxidize the nitrogen oxide, producing nitrogen dioxide and free energy. The release of energy is in the form of visible light (green), and its presence indicates that free oxygen atoms are being produced faster than the rate at which nitrogen dioxide is being introduced. When nitrogen dioxide is introduced at a rate equal to or exceeding the free oxygen atom production rate, the green glow downstream of nitrogen dioxide introduction point is extinguished. When titrating in a darkened room, increasing the nitrogen dioxide flow rate causes the trailing edge of the glow to progress upstream, approaching the point of nitrogen dioxide introduction. This glow becomes sharper and more distinct until it appears to become truncated at the cross-sectional plane defined by the introduction of the nitrogen dioxide titrant. Under these conditions, the nitrogen dioxide flow rate exactly equals the oxygen atom flux through the plane of titration. Wherein, all the oxygen atoms are scavenged by reaction one as they cross the plane of titration, and no free oxygen atoms pass through the plane of titration since reaction two is not observed to occur in the downstream region. This condition is called the titration

end-point, which is highly reproducible and requires only visual observation. Thus, by measuring the nitrogen dioxide flow rate, the free oxygen atom flux can be inferred. By providing a mechanical system which permits positioning of the titration probe at any location downstream of the discharge, free oxygen atom flow rates can easily be measured for any particular cross-sectional plane down stream of the plasma. The percent of oxygen molecules converted to oxygen atoms (dissociation) existing at any particular cross-sectional plane downstream of the discharge can be calculated as one half of the flow rate of oxygen atoms divided by the initial molecular oxygen flow rate (as read off the oxygen supply rotometer). This ratio is denoted as percent conversion throughout the text (Figures 10-15 show typical data).

4.5 Emission Spectra

4.5.1 Visible

At plasma pressures above one torr, neutral species emission spectra of atomic oxygen and atomic hydrogen were observed (See Table 1). When the plasma system was operated at high power and low pressures (0.05 to 1.0 torr), the plasma exhibited a bright white color. A spectral scan from 4500 Å to 6500 Å was performed under these conditions which revealed broad band emission (see Table 2). Brake[6] identified these molecular emission spectra as being the first negative band of oxygen. From the first seven lines of the Q4 branch within each of the three vibrational bands examined, Brake[6] calculated an average gas temperature of 320 K. This seemed to be in direct contradiction to Brake's model. The model predicts bulk gas temperatures of 1000 to

2000 K. The disparity is believed to lie in the operating procedures under which the data was collected. Low pressure operation (0.05 to 0.5 torr) could only be achieved by throttling the oxygen supply flow to near zero. Under limited flow conditions the quartz containment tube became glowing hot. The quartz was observed to have experienced some softening and vitrification (softening of quartz is reported to occur at approximately 1938 K[16]). As a result, forced air was directed over the outside of the containment tube to provide auxiliary cooling. Under low flow conditions, gases undergoing surface-recombination at the containment tube wall should exhibit temperatures corresponding to the wall temperatures. However without auxiliary cooling, wall temperatures (softening and vitrification of the quartz) correspond very well with predicted bulk gas temperatures.

4.5.2 Infrared

After repeated attempts to measure the 1.27 μm emission of $O_2(^1\Delta_g)$ without success, it was concluded that virtually all of the microwave energy was producing neutral excited species atomic oxygen versus neutral excited molecular species. In fact, typically during NO_2 titration the characteristic O-NO glow could be seen throughout the experimental apparatus, indicating the existence of free atomic oxygen; oxygen atoms are a known scavenger of O_2 ($^1\Delta_g$). The half life of O_2 ($^1\Delta_g$) has been measured to be approximately 45 minutes[17] and can typically survive 10^6 wall collisions[18] without deactivation. As a consequence, it is clear that a catalytic device of some sort (Platinum or Nickel wire or a Mercury Oxide coating) should have been employed

upstream or within the cavity to remove O-atoms and hence, preserve the O_2 ($^1\Delta_g$).

The only molecular band structure observed, was the first negative band of oxygen (O_2^+). It was postulated that its formation was by surface-recombination of a neutral oxygen atom and a singly ionized oxygen atom rather than by direct generation. This mechanism accounts for two phenomena: (1) the general lack of excited neutral molecular species as seen in wide spectral scans, and (2) the visual and experimental conditions under which O_2^+ was observed (the plasma changed colors from a deep reddish-purple to bright white at low pressures). The bright white color was attributed to the broad band emission of the singly ionized oxygen molecule.

4.5.3 Stark Broadening

Stark broadening measurements are usually performed on high density/high temperature plasmas. The broadening of the hydrogen β-line (4861 Å) is a result of the electromagnetic interactions of the free electrons surrounding the excited hydrogen species. The extent to which the hydrogen β-line is broadened, is characterized by the electron density within the discharge.

Hydrogen β-line measurements conducted at 650 watts power and pressures of 0.1, 0.7, 2.6, 3.6, 4.6, 6.0, 8.0, 10.0, 12.0, 14.0, 16.0, 18.0, 20.0, 25.0 and 50 torr using the scanning monachrometer revealed a constant line width, Full Width Half Maximum (FWHM) of 0.30 Å. These measurements were taken with the current to voltage converter on the two most sensitive scales. When the measurement was repeated with the Fabry-Perot interferometer in place, the signal was undetectable. Repeated efforts were unsuccessful in producing the sought-for signal with the Fabry-Perot interfometer in place. It is believed that even though some gas may be ionized at very low pressures (0.2 mm Hg) the Hydrogen β-line width is not measurably effected by Start Broadening over the range of plasma densities examined.

CHAPTER 5

RESULTS

5.1 Observations

The data presented in Figures 10 through 15 illustrate the effects of varying pressure, power and flow rates on free oxygen atom production. The range of parameters presented are 8 to 16 torr, 0.4 to 4.0 standard cc/sec and 200 to 600 watts of absorbed power.

Mearns and Morris[3] suggested that it would be interesting to determine the oxygen atom concentration at the exit of the discharge. This was tried, but because the titrant was injected radially from the center of the circular exit plane, the titration end-point could not be achieved without adversely affecting the plasma (introducing NO_2 into the resonant cavity). The oxygen atom flux was a maximum at the exit plane, requiring peak titration flow rates. Under unusually high titrant flow conditions, the titrant would exit the titration probe tip, traverse the radius of the quartz containment tube, strike the tube wall and run both up and downstream. It is noted that if the titrant runs upstream at this location, it is flowing into the resonant cavity where it may undergo dissociation.

The titration data was measured from the exit of the discharge and not from the end of the plasma. The plasma had a tendency of extending beyond the cavity at pressures of less than 14 torr. A maximum titrant flow rate could be anticipated by assuming that 100% of the molecular

oxygen supplied to the resonant cavity underwent dissociation. For an oxygen flow rate of 1.39 ml/sec a maximum time rate of change of titrant pressure was calculated (6.0 torr/sec). If one extrapolates the data curves of Figure 10 back to 1 cm, it is observed that the time rate of change in pressure is greater than the calculated maximum for pressures less than 14 torr. Consequently, if the raw data is corrected by the distance that the plasma extended beyond the resonant cavity, then it appears that there was near 100% dissociation at the pressures where the titrant flow rate equals the theoretical maximum. The highest conversion actually measured was 70% at 12 torr with a 0_2 flow rate of 0.4 cc/sec and 500 watts of absorbed power. Oxygen atom recombination profiles are presented in figures 11 through 13. These figures indicate that for a fixed distance downstream of the discharge, lower pressures produce higher dissociation ratios. Battey[1] and Bell and Kwong[2] found a similar behavior.

Figure 13 compares the yield (gm-atom/kw-hr) of atomic oxygen as a function of locations downstream of the discharge. The data indicates that the yield is highly dependent upon system pressure and distance (as measured downstream of the discharge). The observed trend is that lower pressures produce higher yields for fixed distances downstream of the discharge. Note: it is not correct to assume that the yield is constant. Figure 13 indicates that an error of two orders of magnitude could be made if the yield is measured and calculated at 8 cm downstream of the discharge versus 3 cm. Although Bell and Kwong[2] base their exit plane yield on a single titration point in the effluent of the discharge, they do report a similar overall trend.

The direct measurement technique utilized within this experiment eliminated the need to extrapolate yields for various locations downstream of the discharge, and as a consequence, the direct mapping of the recombination profile could be determined.

Battey[1] found that at one (1) torr, higher flow rates produced the same amount of conversion as the lower flow rates. He concluded that at the lower flow rates, more of the oxygen atoms had undergone surface recombination prior to the time the gas had reached the titration port. He also expected the oxygen atom concentration would drop off for higher flow rates, due to the lower residence time (the amount of time the oxygen gasses spend within the discharge). In this experiment, varying the oxygen supply gas flow rate was observed to have a small, but measurable, effect on oxygen conversion (see Figure 14). The conversion varied at most 11% over a seven-fold change in supply gas flow rate. Note that the conversion curve (Figure 14) displays a minima at about 27% at approximately 0.7 cc/sec. This seems to suggest that there must be at least two independent mechanisms which are both influenced by the flow rate. It is suggested that the two competing mechanisms are (1) gas residence time, and (2) oxygen atom recombination kinetics. Clearly, equilibrium dissociation levels established within the reactor are a function of these phenomena. The longer the gas spends within the discharge, the higher the available energy per molecule to dissociate and excite the atom. The more complete the dissociation, the higher the concentrations are which drive recombination reactions.

Some information can be gained by examining the yield curve plotted in Figure 14. It is noted that for each increase in flow rate, the yield increases. The yield (gm-atom/kw-hr) can be thought of as an efficiency measurement. The system continually becomes more efficient with increasing oxygen flow rates. The conversion is noted to decrease over the flow rate range of 0.0 to 0.7 cc/sec, since the transient time (the time the gas travels from the exit of the plasma discharge to the location of analysis) is on the order which permits measurable decreases in conversion as a result of the recombination kinetics (both wall and third-body collisional deactivation). As the flow rate is further increased (0.7 to 1.2 cc/sec), the gas transient times continue to decrease. Ultimately, this leads to shorter and shorter reaction periods for the oxygen atom recombination kinetics, wherein the oxygen atom recombination reaction does not reach the same degree of completion prior to analysis. As a result, highest conversions and yields are measured at the highest flow rates for the fixed titration point case.

Eventually, a turning point must exist, where increasing molecular oxygen flow rates decreases atomic oxygen yield. This point is identified as being when the oxygen mass flow rate is sufficiently high such that maximum dissociation is no longer attained for the fixed power supplied. This behavior is characterized in the data presented in Figure 15. For a fixed pressure, flow rate and analysis point the yield increases rapidly with power. For high powers (greater than 500 watts) the rate of increase in yield drops off. This could be seen as reaching a saturation (100% dissociation) where further increases in power do not contribute to increases in yield but may contribute to increased excited species population and/or gas temperatures. This limitation accounts

for the asymptotic nature of the yield curve in Figure 15. The conversion is observed to increase at a near linear rate with power.

CHAPTER 6

Conclusions

6.1 Summary

High molecular oxygen dissociation ratios were observed downstream of the microwave (2.44 GHz) discharge for pressures of 1-16 torr, a net power range of 200-600 watts and molecular oxygen flow rates of 0.4 to 4.0 cc/sec. The oxygen recombination profiles, which were generated by titrating the effluent gasses with nitrogen dioxide, in general, indicated that decreases in plasma pressure or increases in absorbed power and/or oxygen flow rates produced an increase in atomic oxygen concentration. These results were consistent for each particular cross-sectional plane downstream of the plasma discharge.

6.2 Comparison of Experimental Method

The initial experimental apparatus utilized pepper pot nitrogen dioxide injectors located considerable distances downstream of the plasma discharge (13, 31 and 83 cm). The nozzle was designed based on similar arrangements by previous authors (References 1, 2, 3, 19, and 20). The pepper pot nozzles could be pointed either upstream or downstream since they were connected to the analytical flow regime by ground glass joints. The problem identified with such an arrangement was that if one pointed the injectors upstream the titration endpoint was difficult to ascertain. This was due to the fact that the titrant was reacting at some undeterminable distance upstream of the nozzle. If the

nozzles were turned downstream, the reaction was taking place in the wake of the injector itself. The additional problems associated with poor reagent mixing and surface recombination deemed it imperative not to perform titration measurements in the wake of the pepper pot injector. As a result the sliding proble technique developed here proved invaluable in gathering titration data throughout the analytical flow regime.

6.3 Proposal for Additional Research

6.3.1 Analytical

Several measurements should be performed which time did not permit.

First, bulk gas temperature measurements as a function of supply gas flow rates and power should be performed. The research presented within this text was initially conducted under the assumption that gas temperatures remained essentially at room temperatures. Many of the observations presented herein indicate that bulk gas temperatures are indeed at elevated temperatures.

Second, gas velocity measurements as a function of power and distance downstream of the discharge should be performed. Recombination reaction rates could be determined which could be compared with those values within literature and to better understand the significant components within the recombination process.

Third, spectral information should be gathered as a function of flow rates (discharge resident time). This single measurement could explain much of the uncertainties associated with discharge resident time.

6.3.2 Experimental

The single biggest improvement which could have been made in the experimental apparatus is the employment of a real time titration system. The titration system described herein utilizes a time rate of change of pressure in an isolated volume to determine titrant flow data, data collection proved to be tedious and time consuming. The employment of digital flow transducers would enable the experimentalist to generate smooth curves, directly, with maximum knowledge and control of the conditions under which the data is being collected.

Secondly, some effort should be made to further optimize the experimental apparatus so as to match the coaxial input probe impedance with the resonant cavity. Although cavity tuning minimized reflected power, unique plasma characteristics were exhibited under near-matched impedance conditions.

Third, due to the many different plasma distributions which were observed, specific effort should be directed towards characterizing the various power coupling modes.

REFERENCES

1. J. Battey, "Design Criteria for Uniform Reaction Rates in an Oxygen Plasma", IEEE Trans on Electron Devices 24, 140, 1977.

2. A. Bell and K. Kwong "Dissociation of Oxygen in a Radiofrequency Electrical Discharge", AICHE 18, 990, 1972.

3. A. Mearns and A. Morris, "Oxidation Reactions in a Microwave Discharge: Factors Affecting Efficiency of Oxygen Atom Production", Chem Eng Prog Ser 112, 37, 1971.

4. F. D. Francis, "The Production of Oxygen Atoms in a Microwave Discharge and the Recombination Kinetics in a Gas Flow System", J Appl Phys 2, 1717, 1969.

5. R. McCarthy, "Chemical Synthesis from Free Radical Production in Microwave Fields", J Chem, Phys 22, 1360, 1954.

6. M. L. Brake, R. L. Kerber, "Dissociation and Recombination of Oxygen Atoms Produced in a Microwave Discharge, Part II: Theoretical Calculations", Plasma Chemistry and Plasma Processing, Volume 3, No. 1, 1983.

7. Zeidel, Prokoter et al, Table of Spectrum Lines, IFI/Plenum Data Corp, New York, 1970.

8. J. Asmussen, R. Mallavarpu, J. Hamann and H. Park, "The Design of a Microwave Plasma Cavity", Proc IEEE 62, 109, 1974.

9. H. Griem, Spectral Line Broadening by Plasmas (New York: Academic Press, 1974).

10. H. Griem, Plasma Spectroscopy (New York: McGraw Hill, 1964).

11. W. Lochte - Holtgreven, Plasma Diagnostics (Amsterdam: North Holland Pub, 1968).

12. G. B. Kistiakowsky and G. G. Volpi, "Reactions of Nitrogen Atoms I Oxygen and Oxides of Nitrogen", J Chem Phys 27, S, Nov 1957.

13. R. Kerber and A. McKnight, Private Communication AFWL Kirtland AFB, Albuquerque, New Mexico (1973).

14. J. Greaves and J. Linnett, "Recombination of Atoms at Surfaces", Trans Farad Soc 54, 1355, 1961.

15. J. Linnett and D. Marsden, "The Kinetics of Recombination of Oxygen Atoms at a Glass Surface", Proc Roy Soc S234, 489, 1956.

16. I. E. Campbell, High Temperature Technology, Electrochemical Society, John Wiley and Sons, 1965.

17. R. M. Badger, A. C. Wright and R. F. Witlock, J. Chem Phys, 43, 4345 (1965).

18. J. A. Davidson and E. A. Ogryzlo, Chemiluminescence and Bioluminescence. Plenum, New York, 1973.

19. P. Kocian, Phys Letts 73A, 11, 1979.

20. F. Kaufman, "The Air Afterglow and its Uses in the Study of Some Reactions of Atomic Oxygen", Proc Roy Soc London, A247, 123, 1958.

TABLE 1

Observed Spectral Lines of Atomic Oxygen

Wavelength Å	Multiplet
3947.3	$3s^5S^0 - 4p^5P$
4368.3	$3s^3S^0 - 4p^3P$
5329.0	$3p^5P - 5d^5D^0$
5436.8	$3p^5P - 6s^5S^0$
6046.4	$3p^3P - 6s^3S^0$
6157.3	$3p^5P - 4d^5D^0$
6455.0	$3p^5P - 5s^5S^0$
7156.8	$3s^1D^0 - 3p^1D$
7254.4	$3p^3P - 5s^3S^0$

TABLE 2

Observed Band Heads
of the First Negative System of O_2^+

Wavelength Å	Transitions v" - v'
6419.2	0 - 1
6351.1	1 - 2
6291.9	2 - 3
6232.7	3 - 4
6177.2	4 - 5
6026.4	0 - 0
5973.5	1 - 1
5925.7	2 - 2
5883.5	3 - 3
5847.4	4 - 4
5814.4	5 - 5
5631.9	1 - 0
5597.6	2 - 1
5566.7	3 - 2
5540.8	4 - 3
5520.9	5 - 4
5295.7	2 - 0
5274.7	3 - 1
5259.2	4 - 2
5251.2	5 - 3
5241.0	6 - 4

TABLE 3

Calculated Resonant Cavity Modes for an Evacuated Cylinder (178 mm ID)

Electromagnetic Modes	Calculated Short Position	Radial Probe Position (mm)*
TE_{111}	67	68
TM_{011}	72	72
TM_{211}	82	76
TE_{011} & TM_{111}	112	72
TE_{112}	134	75
TM_{012}	144	72

*Experimately observed maximum coupling probe position. Probe position was measured from the tip of the coaxial probe to the I.D. surface of the cylindrical cavity.

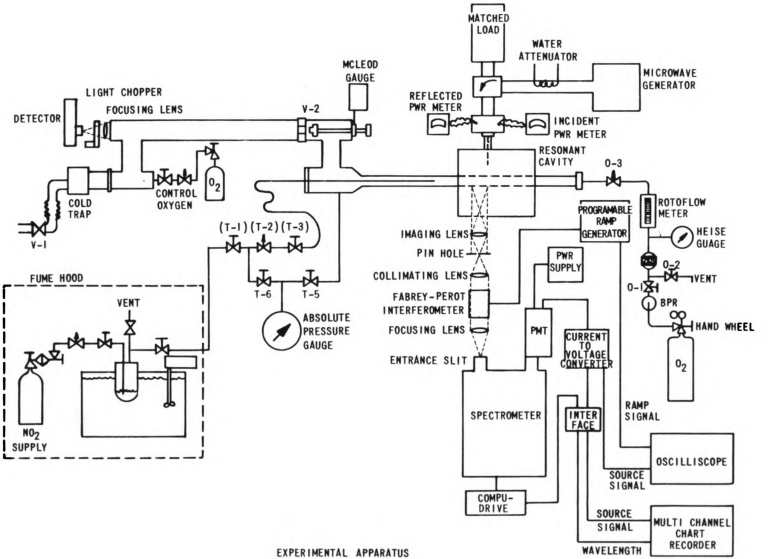

EXPERIMENTAL APPARATUS

FIGURE 1

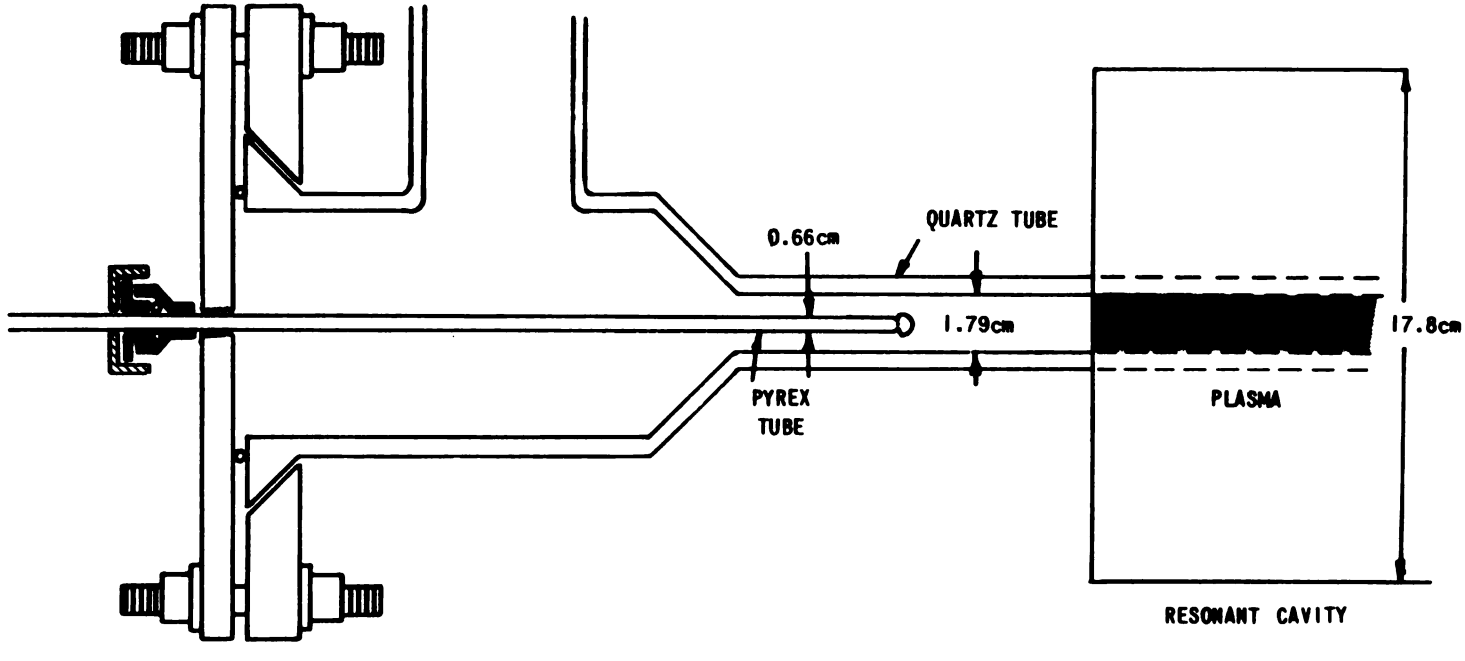

MOVABLE TITRATION PROBE
FIGURE 2

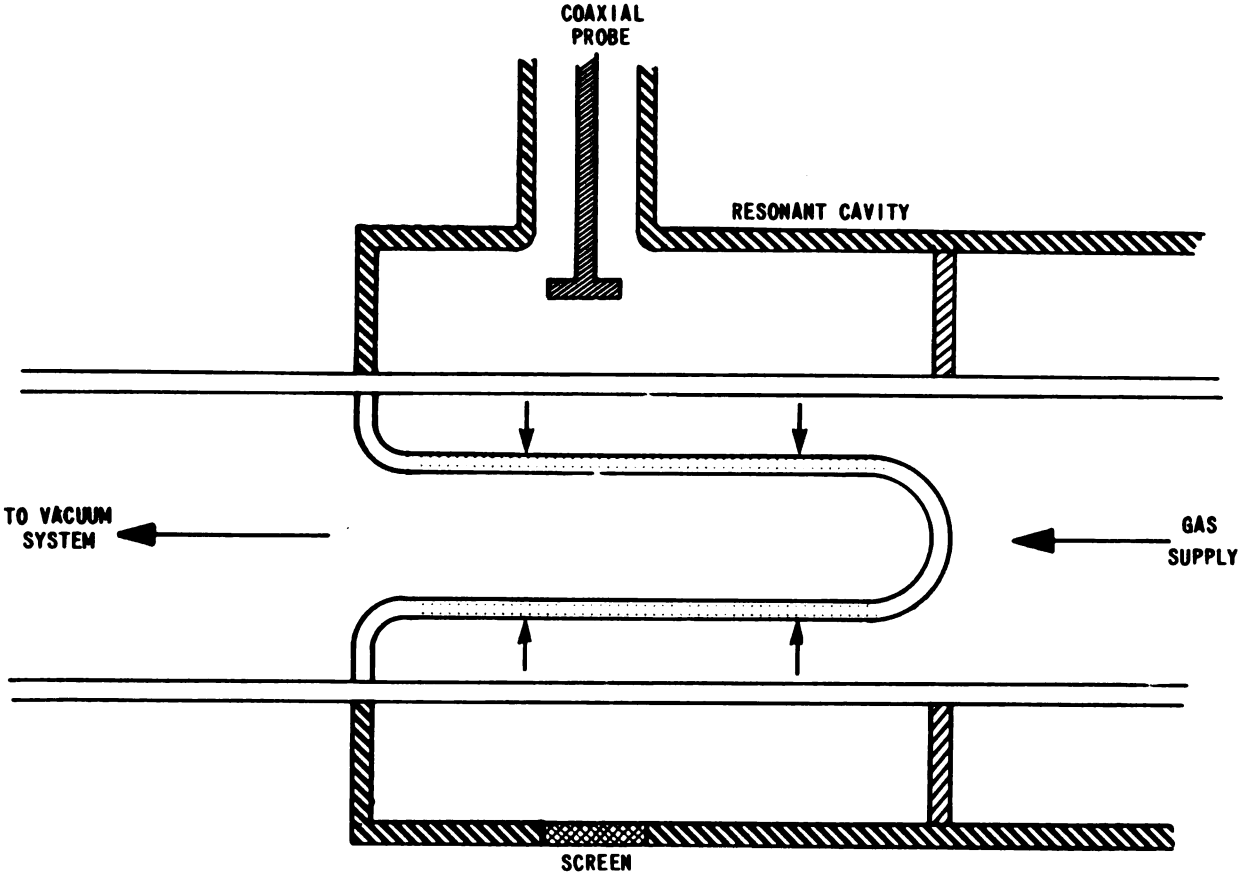

RADIAL FLOW TUBE
FIGURE 3

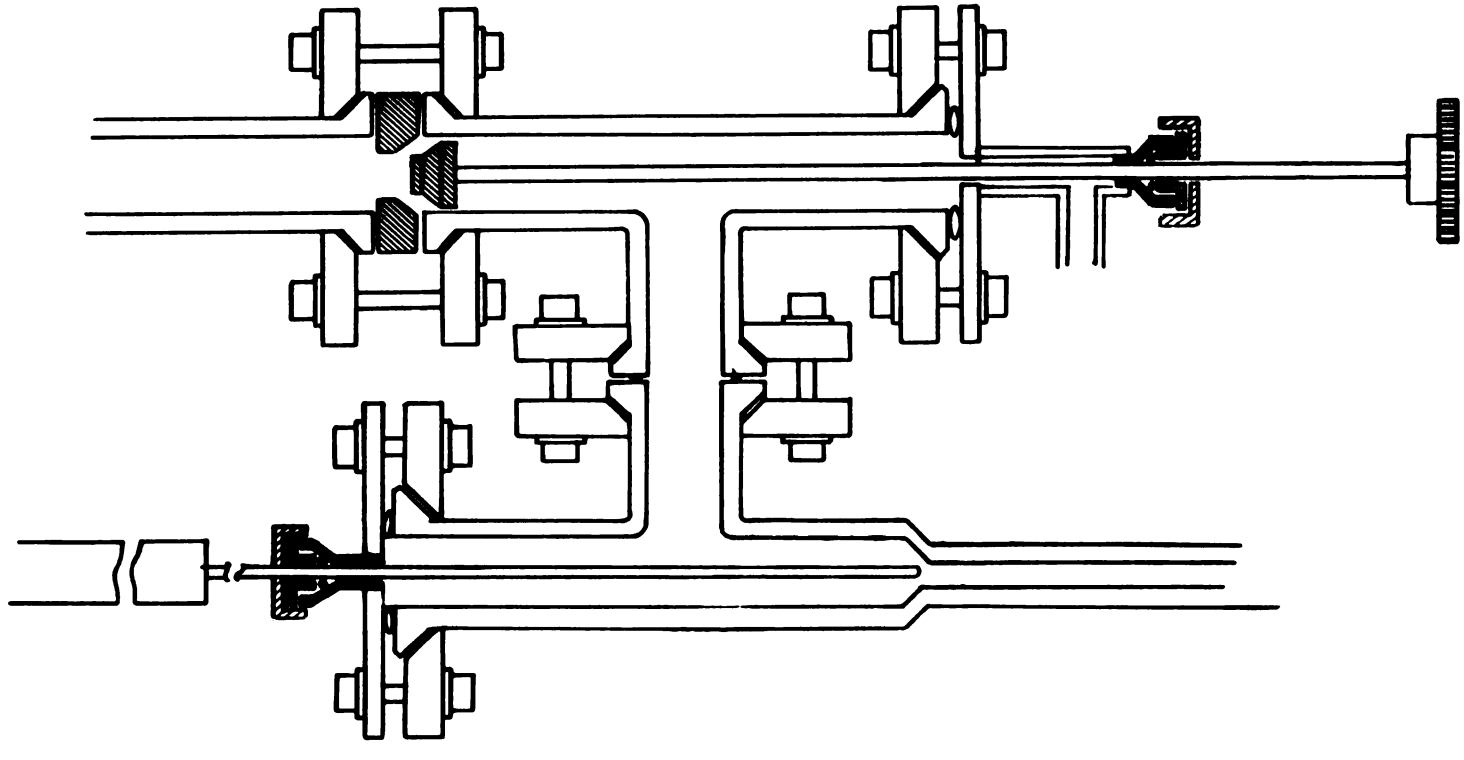

SYSTEM ISOLATION VALVE
FIGURE 5

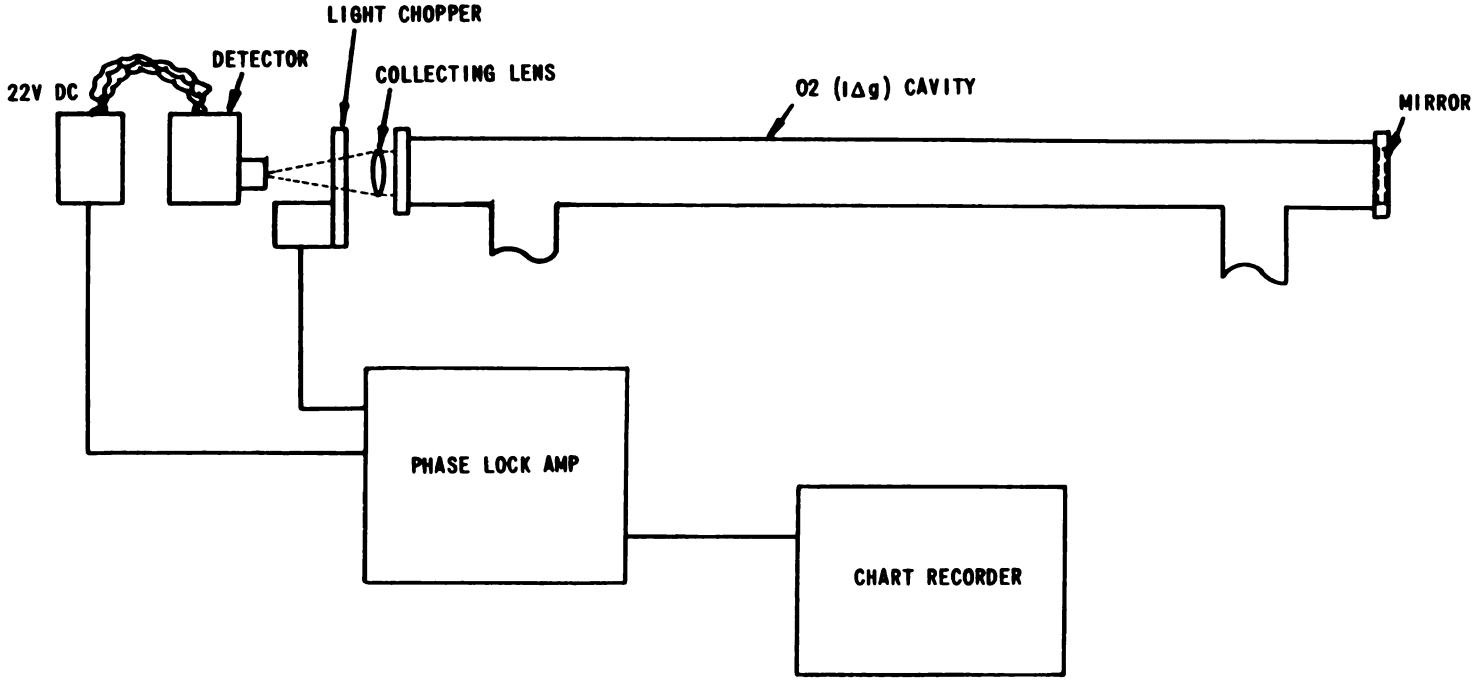

O2 (1Δg) APPARATUS

FIGURE 6

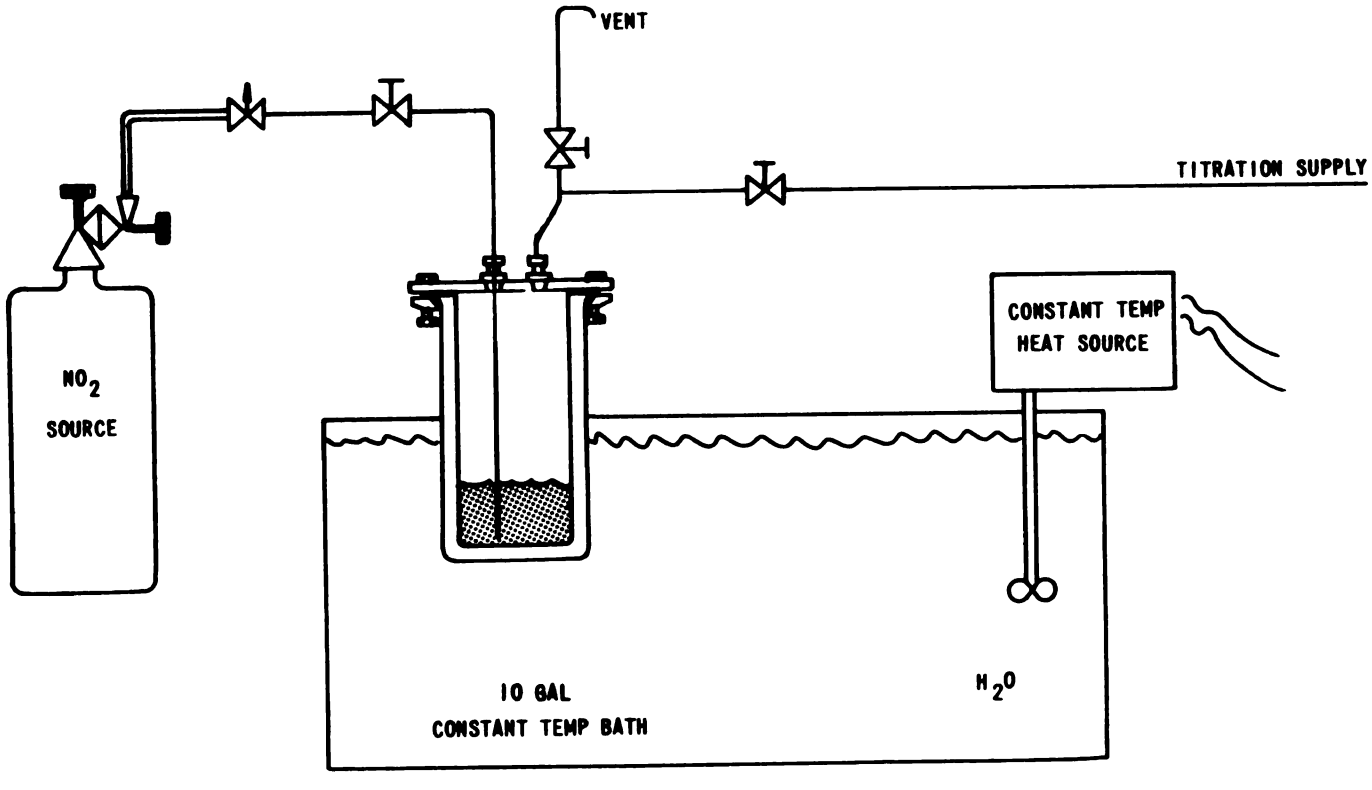

NITROGEN DIOXIDE SUPPLY SYSTEM
FIGURE 7

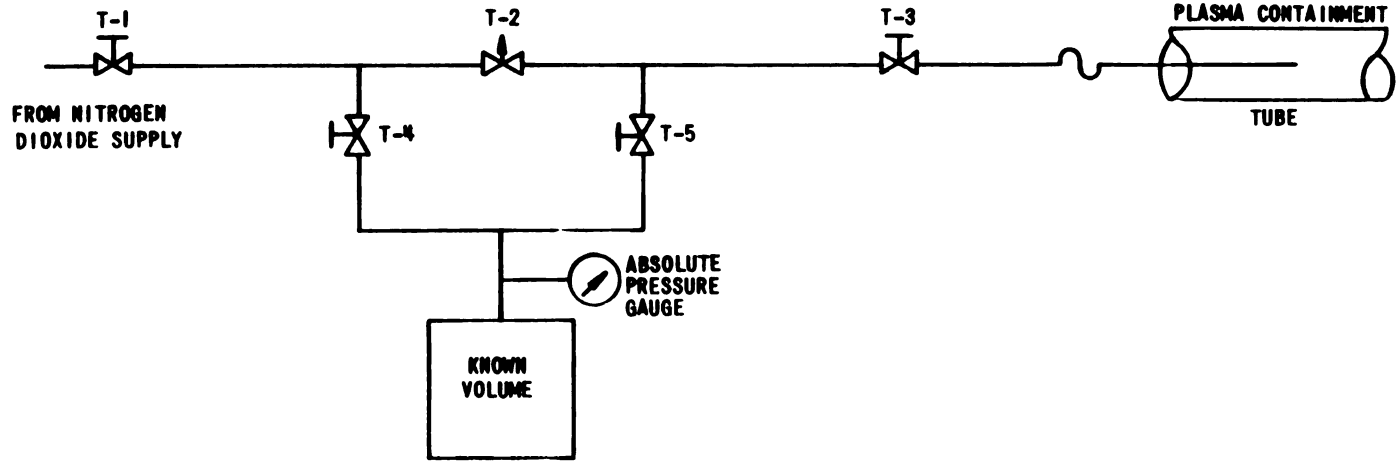

FIGURE 8a

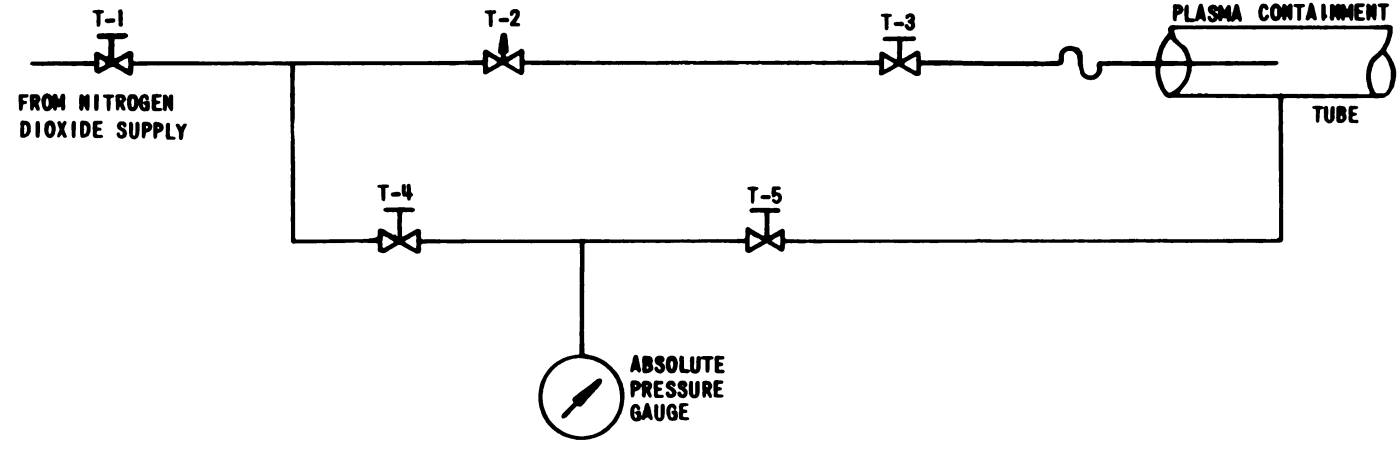

TITRATION STATION
FIGURE 8b

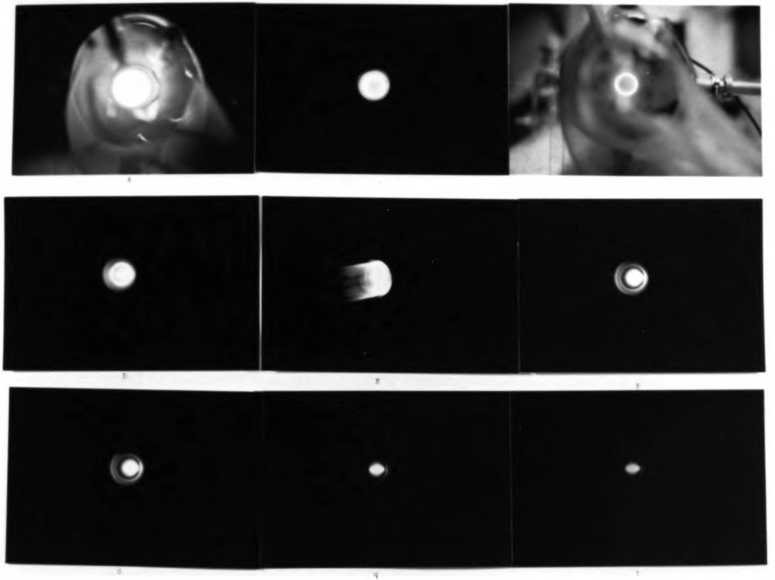

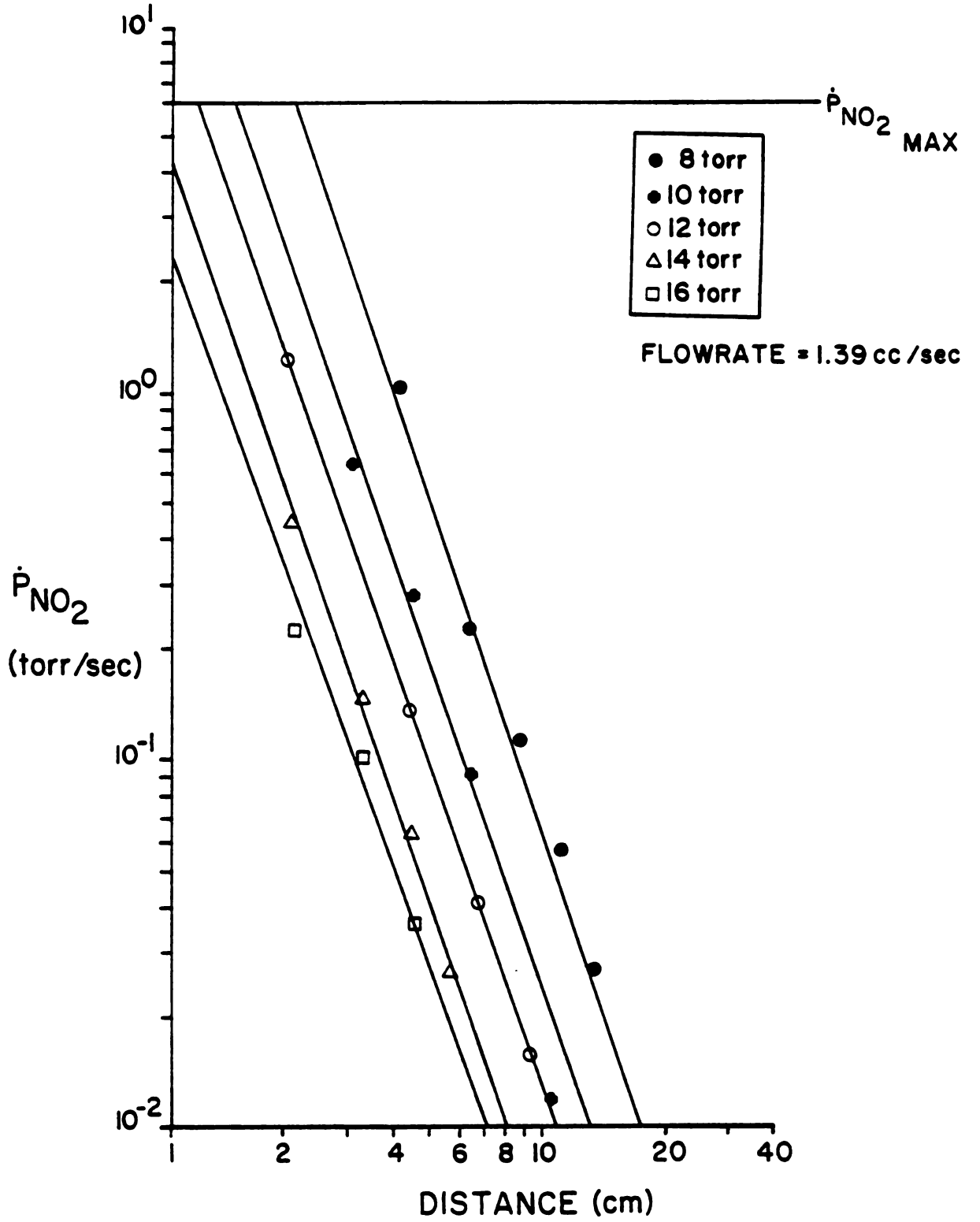

Figure 10 The Effect of Distance on $\dot{P}_{NO_2}$ for Several Pressures

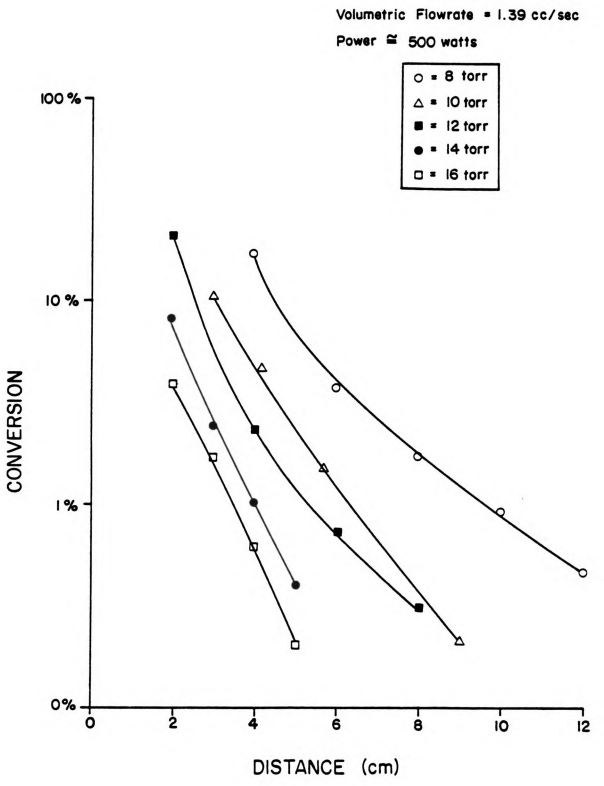

Figure 11 Molecular Conversion vs Distance From the Exit of the Reactor Cavity for Various Pressures

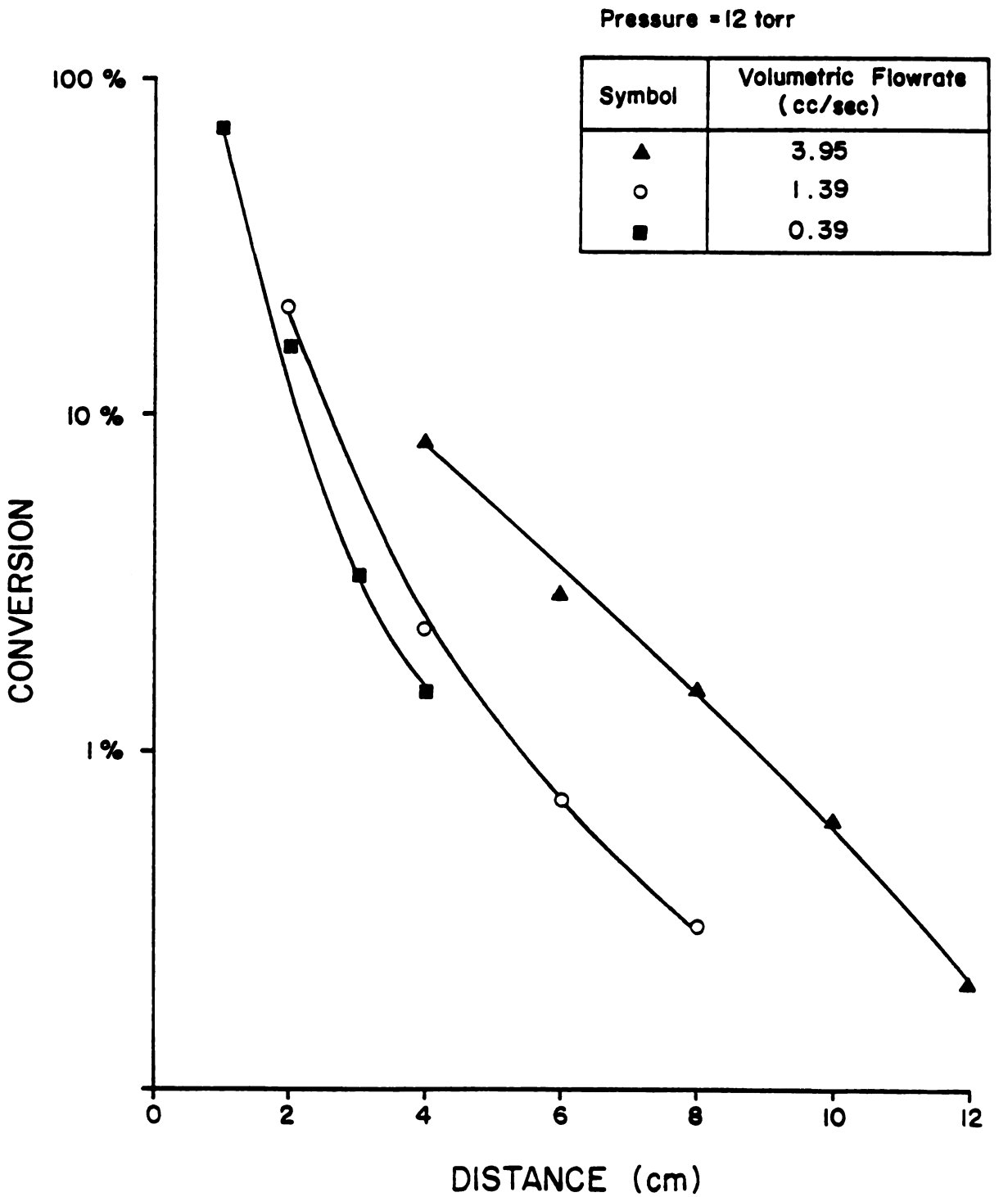

Figure 12 Molecular Conversion vs Distance for Various Flowrates

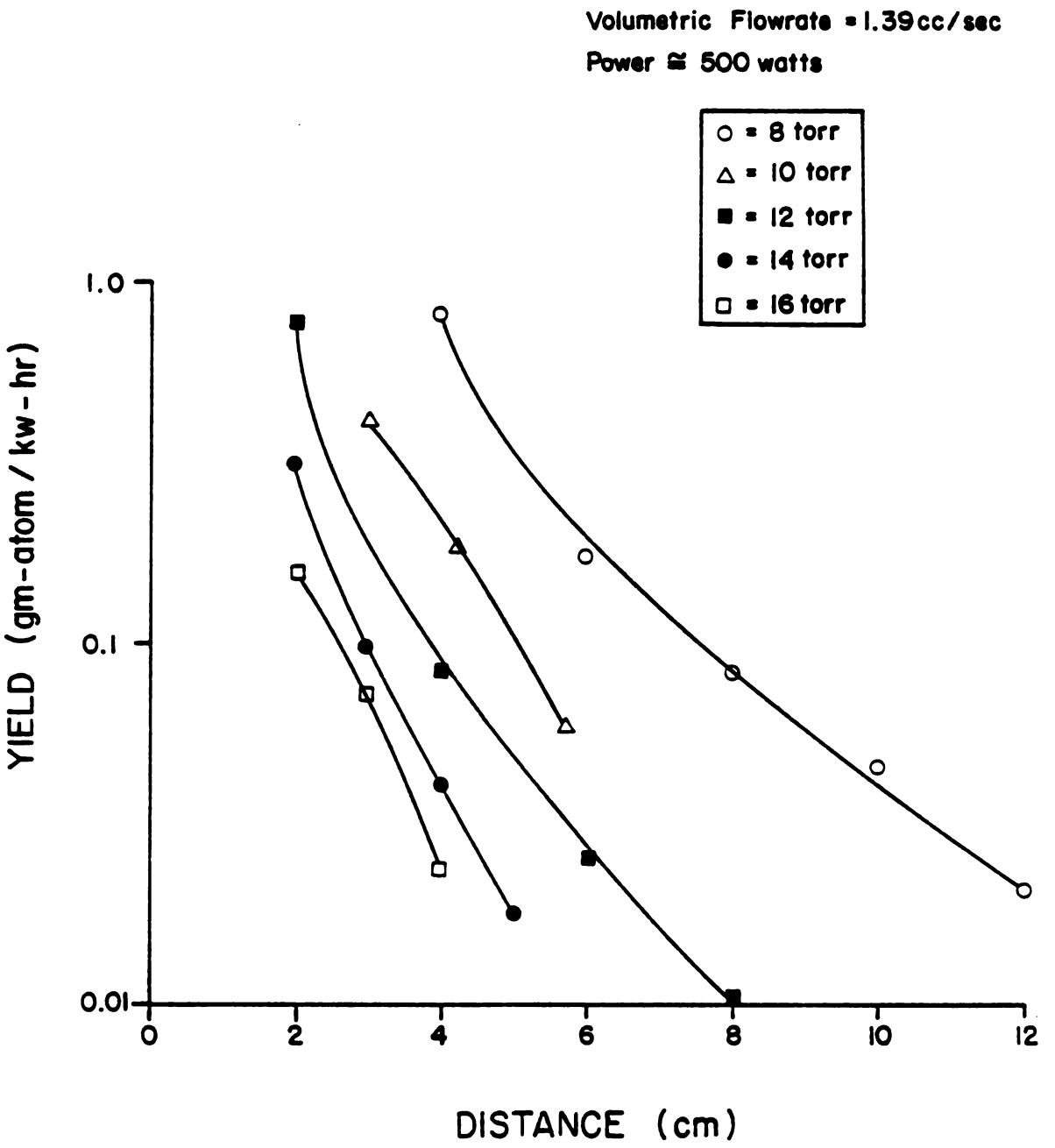

Figure 13 The Number of Atoms Per Unit Energy (Yield) Produced vs Distance

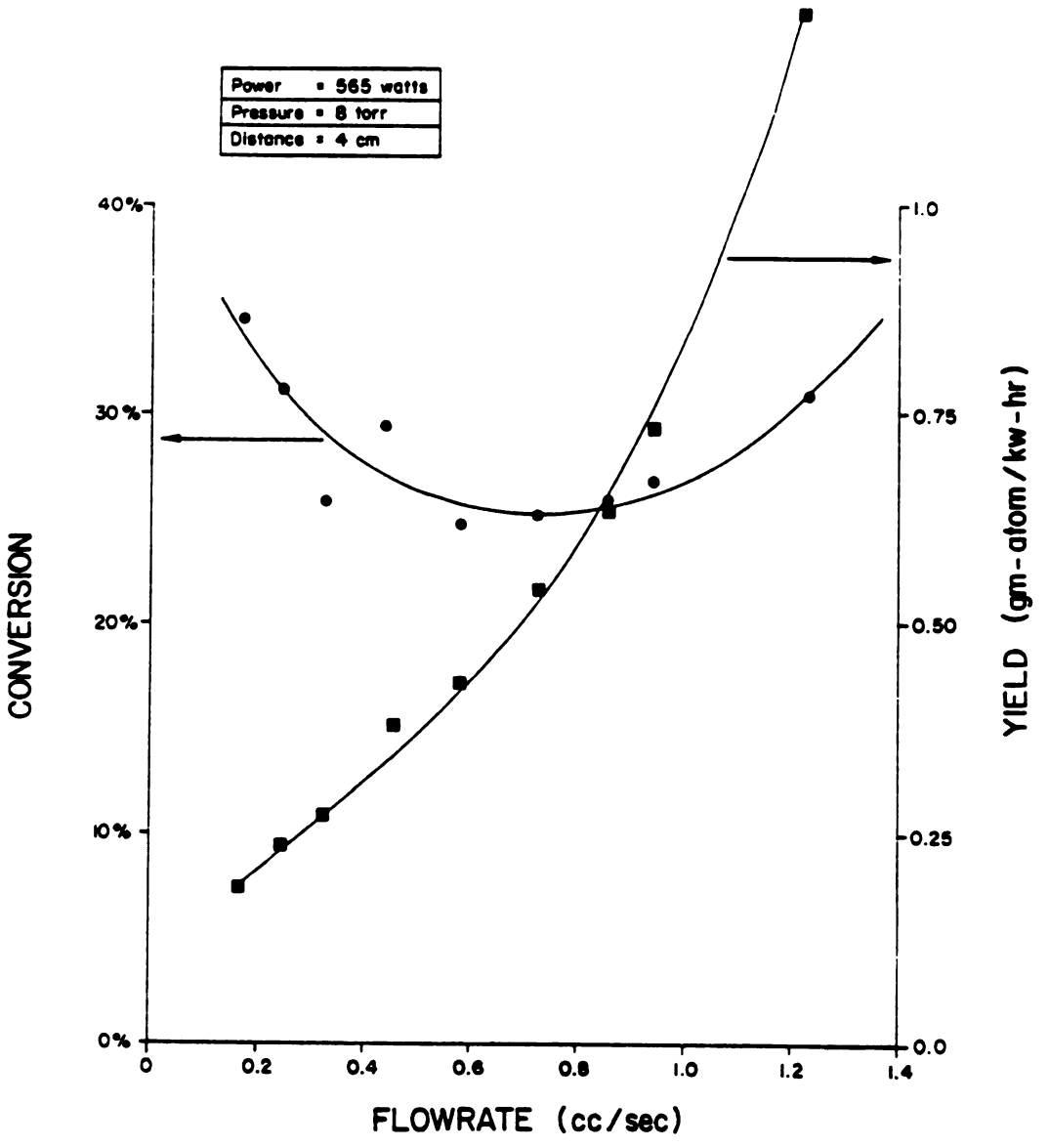

Figure 14 Oxygen Atom Yield and Molecular Conversion vs Flowrate

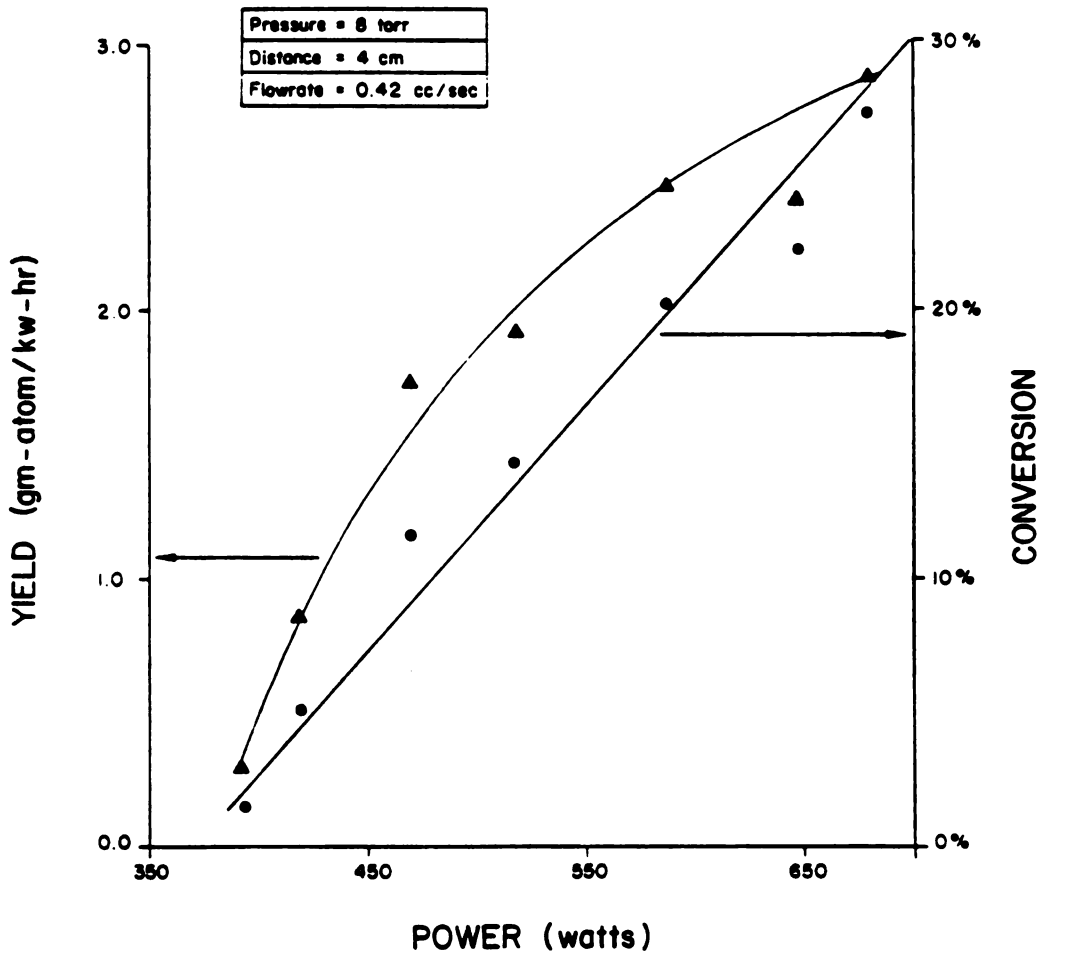

Figure 15 The Effect of Power on Oxygen Atom Yield and Oxygen Molecule Conversion